Real-time feedback controlled conversion in vat photopolymerization of ceramics

Additive Manufacturing 30 (2019) 100775

Contents lists available at ScienceDirect

Additive Manufacturing

journal homepage: www.elsevier.com/locate/addma

Real-time feedback controlled conversion in vat photopolymerization of ceramics: A proof of principle☆

Thomas Hafkamp[a,b,*], Gregor van Baars[b], Bram de Jager[a], Pascal Etman[a]

[a] Department of Mechanical Engineering, Eindhoven University of Technology, Eindhoven, The Netherlands
[b] Department Equipment for Additive Manufacturing, TNO, Eindhoven, The Netherlands

ARTICLE INFO

Keywords:
Stereolithography
Closed-loop process control
In-situ process monitoring

ABSTRACT

Technical ceramics for high-performance applications can be additively manufactured using vat photopolymerization technology. This technology faces two main challenges: increasing ceramic product size and improving product quality. The integration of process control strategies into AM equipment is expected to play a key role in tackling these challenges. This work demonstrates the feasibility of real-time and in-situ feedback control of the light-initiated polymerization reaction that lies at the core of vat photopolymerization technology. To prove the principle, a single-layer experimental setup was developed in which the degree of conversion was measured by infrared spectroscopy. Experimental data obtained from this setup was used to develop a control-oriented process model and identify its parameters. A material perturbation was applied by adding an inhibitor and the case with and without feedback control were compared. The results show that the feedback controller successfully compensated for the material perturbation and reached the same final conversion value as the unperturbed case. This result can be considered a fundamental step towards additive manufacturing of defect-free ceramic parts using in-line process control.

1. Introduction

Additive Manufacturing (AM) opens the door to enhanced product functionality and performance [1], irrespective of the material used. Manufacturing near-net shape parts from high-performance ceramic materials, however, is generally challenging [2]. Current applications of ceramic AM already include bone implants, waveguides, and investment casting cores [3,4], but these components are relatively small. Future applications in the high-tech industry require build volumes to expand to around one cubic meter. This expansion will enable the fabrication of large structural machine components, such as exposure stages for the semiconductor industry [5].

The machine component designer has several options at hand to additively produce ceramics, one of which is vat photopolymerization [2,4]. Vat photopolymerization was initially developed to fabricate pure polymers [6] and later to produce green bodies for polymer-derived ceramics [7]. To this end, a mixture of ceramic particles and photopolymer resin is selectively cured in an AM machine, followed by polymer burn-out and ceramic particle fusing in a furnace. From an equipment perspective, nothing changes in the photopolymerization working principle when unfilled photocurable resins are replaced by ceramic-filled slurries. From a rheological or optical perspective, however, adding ceramic materials changes the material properties. This property change makes ceramic slurries more difficult to process than pure polymers. Moreover, the formation of cracks or other defects in the ceramic product can cause inadequate quality or even complete rejection.

Improving product quality and scaling up to large areas calls for advancements in vat photopolymerization equipment and control architecture. To work towards these advancements, one can view the AM machine as a mechatronic system and pursue developments in process modelling, sensing, actuation and control action computation as depicted in Fig. 1. This approach can be followed for both the major process steps: material supply through recoating [8] and material transformation through photopolymerization [9]. Both process steps need to transition from open-loop to closed-loop control to minimize the sensitivity to equipment, material and process variability [10,11].

Closed-loop (feedback) control is hardly addressed in literature for both the major process steps in vat photopolymerization. On the contrary, decades of work has been published on photopolymerization or

☆ No author associated with this paper has disclosed any potential or pertinent conflicts which may be perceived to have impending conflict with this work. For full disclosure statements refer to https://doi.org/10.1016/j.addma.2019.06.026.

* Corresponding author at: Department of Mechanical Engineering, Eindhoven University of Technology, Eindhoven, The Netherlands.
E-mail addresses: t.m.hafkamp@tue.nl, thomashafkamp@me.com (T. Hafkamp).

https://doi.org/10.1016/j.addma.2019.06.026
Received 30 April 2019; Received in revised form 19 June 2019; Accepted 30 June 2019
Available online 08 July 2019

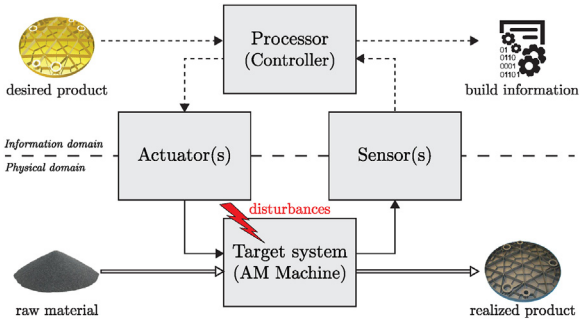

Fig. 1. Mechatronic system view of an AM machine.

cure *monitoring* [12], which is the process of observing, tracking, and analyzing information about the process to ensure that the process is on-course in meeting performance objectives. Few researchers have attempted to make the transition from using process measurements merely for process *monitoring* to using them for automatic process *control* [13]. Yebi et al. developed a model-based process control scheme for UV curing of glass fiber composites in which a precomputed surface temperature trajectory was tracked [14–16]. Zhao and Rosen developed a bang-bang control scheme for a layerless photopolymerization process in which the cured height of microparts was controlled [17,18].

Building upon these previous works, control strategies can be conceived for both the recoating and the photopolymerization steps at different length and time scales [9] The applicability of control schemes for the recoating step depends on the specific recoating method, whereas the applicability of photopolymerization control schemes covers a wide area of photopolymerization methods. Since the underlying material transformation principle is the same in all vat photopolymerization systems, this work focuses on the photopolymerization step. Moreover, due to the common working principle, this work is not only relevant for all AM technologies falling into the category of vat photopolymerization, but for virtually any manufacturing technology involving UV curing, including material jetting [1], UV coatings [19], and dental fillings [20].

The works of Yebi et al. and Zhao and Rosen demonstrate that a paradigm shift may be emerging [17] concerning the incorporation of real-time process monitoring and closed-loop control systems into photopolymerization-based AM equipment. The most challenging form of such closed-loop control is arguably real-time in-situ continuous control of the actual material transformation process, i.e., the photopolymerization reaction. Alternatively, ex-situ discrete control strategies can be considered such as cycle-to-cycle [21], layer-to-layer, product, or batch control strategies [22] which were already developed for other AM technologies.

Despite the pioneering works of Yebi et al. and Zhao and Rosen, the implementation of real-time closed-loop control systems in AM machines remains a major challenge. On the one hand, Yebi et al. *indirectly* controlled a one-dimensional (1D) degree of monomer conversion distribution throughout multiple layers by virtue of an estimate from a surface temperature measurement [14–16]. They argue that minimizing degree of conversion and temperature gradients benefits final part quality [16]. On the other hand, Zhao and Rosen controlled the cured height of single-layer parts using an interferometer [17,18], thereby essentially controlling a 1D final part dimension instead of monomer conversion. They argue that the next step is to control not only part *geometry*, but also part *properties* [18].

The realization of voxel-level control of material properties is an elemental target [10] towards controlling both part geometry and final part properties. To this end, the measurable and controllable process parameters need to be identified that influence the final part properties [10]. The degree of monomer conversion is commonly accepted as a well-measurable parameter for the progress of the photopolymerization reaction [12,23] and even can be used to infer material property evolution [24]. Moreover, the degree of conversion is measurable at the sub-voxel scale, so the probing volume is so small that the volume can be considered homogeneous or zero-dimensional (0D) and spatial gradients can be neglected. Contrary to the 1D situations in the works of Yebi et al. and Zhao and Rosen, this 0D situation allows for demonstrating what can be achieved on the microscale by virtue of feedback control when neglecting spatial effects such as light attenuation. The 0D results may serve as a fundamental benchmark for future endeavors to control spatially-distributed photopolymerization. Furthermore, *directly* measuring and controlling the degree of conversion in-situ in an infrared spectrometer eliminates the need for sensor validation, since it is considered a reliable technique to measure conversion [12,23].

Although monitoring the photopolymerization step is a matured field, the sensing aspect seems to be the most critical for real-time control feasibility, whereas the actuation aspect by light fortunately seems to form no fundamental limitation [9]. Future machine integration poses stringent requirements on the sensing aspect. Specifically, it is desired to measure many voxels spanning a large range at high sampling rates, i.e., at high spatio-temporal resolution. Moreover, it is desired to both actuate and measure multiple layers on the same side.

In this work, these challenging sensing requirements are relaxed and a single-input–single-output (SISO) experimental setup is developed. The setup features a single layer and a practically homogeneous UV irradiation field to represent the process at the (sub-)voxel scale. By conducting proof-of-principle experiments on the lab setup, this work aims to demonstrate the feasibility of real-time and in-situ feedback control of monomer conversion in the photopolymerization reaction.

This paper is organized as follows. First, the experimental setup for photopolymerization control is described in Section 2. Sample preparation and the design of the parameter identification and closed-loop control experiments are discussed as well. Second, a control-oriented process model is derived in Section 3. Third, the experimental results are presented in Section 4 followed by a discussion on control feasibility in a large-scale machine setting in Section 5 and concluding remarks in Section 6.

2. Methods

The main working principle of vat photopolymerization is that a photocurable resin is selectively cured through a UV light-initiated polymerization reaction [1,25,26], see Fig. 2. In a highly oversimplified

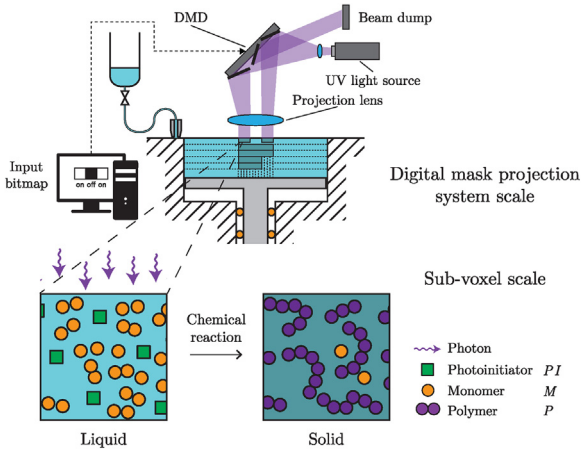

Fig. 2. Main working principle of a vat photopolymerization system: liquid monomer is converted into solid polymer through a light-initiated polymerization reaction. Contrary to vector scanning systems, mask projection systems have a stationary light source (actuator), which allows for a simple SISO system description.

form, this polymerization reaction merely converts an amount of liquid monomer M into a solid polymer P:

$$M \rightarrow P. \tag{1}$$

Certainly, the actual polymerization reaction is much more involved [27,28], but this understanding suffices here. The extent to which this polymerization reaction has progressed, can be quantified by a metric termed the *degree of conversion* α:

$$\alpha(t) = \frac{[P](t)}{[M]_0} = \frac{[M]_0 - [M](t)}{[M]_0} = 1 - \frac{[M](t)}{[M]_0}, \tag{2}$$

where $[M](t)$ and $[P](t)$ are the instantaneous monomer and polymer concentration respectively and $[M]_0 = [M](0)$ the initial monomer concentration.

A control volume containing monomer or polymer can be considered homogeneous or infinitesimally small if the system boundary is drawn on the sub-voxel or micrometer scale. A simple SISO system is obtained if this notion of a zero-dimensional space is combined with the assumption that the polymerization reaction has only one stationary input and one output, i.e., light intensity and degree of conversion respectively.

2.1. Experimental setup layout

Since the degree of conversion is commonly accepted as a good measure for the progress of the reaction [12,23] and even can be used to infer material property evolution [24], this variable is selected as the measured variable in the control system. A multitude of measuring principles are used to measure conversion in *offline polymer characterization equipment*, including calorimetry, dielectrometry, and spectroscopy [9,12,23]. However, measuring the degree of conversion *online* and *in-situ* in the *AM machine* is challenging, let alone at high spatio-temporal resolution.

These challenging requirements were relaxed in this preliminary study, but the requirement for a high spatial resolution was retained to obtain a 0D SISO system. Hence, a measuring technology with a small probing volume needed to be selected. Fourier-transform infrared spectroscopy (FTIR) in attenuated total reflection (ATR) mode was selected, due to its micrometer-sized probing volume and its direct relationship between the measured absorbance and monomer concentration. The FTIR spectrometer (Thermo Scientific Nicolet 6700 with Smart Orbit ATR accessory) served both as the *sensor* and as the *plant* in the control system, since samples had to be applied onto its measuring surface.

To complete the control system, the spectrometer was augmented with a 405 nm UV LED *actuator* (Bivar UV5TZ-405-30) and an *embedded controller* (Raspberry Pi 3 Model B) with MATLAB/Simulink support. Control schemes were implemented in MATLAB/Simulink on a master PC and an ethernet connection between the PC and the embedded controller allowed for initiating experiments and logging data. Fig. 3 schematically shows the layout of the hence obtained embedded control system. Real-time data communication functionality was added to the FTIR spectrometer by self-developed software interfacing with Thermo OMNIC software through the Dynamic Data Exchange (DDE) protocol.

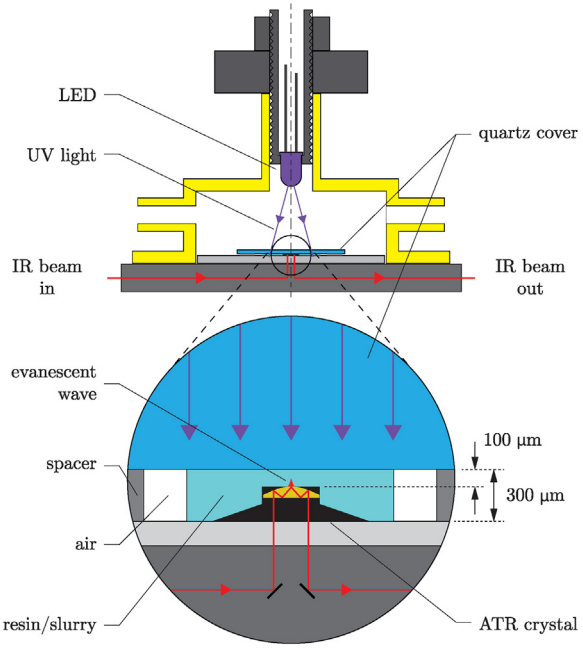

Fig. 4. Schematic layout of the ATR-FTIR experimental setup.

2.2. Sample preparation and materials

Samples were prepared by depositing a droplet of material onto the ATR crystal, placing a 300 µm thick steel spacer around it, and covering with a 1 mm thick quartz window (Thorlabs). The protruding geometry of the ATR crystal makes an impression in the sample as depicted in Fig. 4. Since the protruding height is 200 µm, the resulting layer thickness is approximately 100 µm. Note that of these 100 µm only the bottom few micrometers are probed in the FTIR measurements. Although the UV LED does not yield a homogeneous irradiance field, the irradiance is practically constant in the 3.5 mm diameter ATR crystal area and even more so in the smaller (single-bounce) probing area. The UV light intensity was calibrated using a UV power meter (Delta Ohm HD2302.0, LP471 detector). All experiments were performed under lab conditions at 20 °C room temperature and purposely performed without nitrogen flushing the sample chamber beforehand, to better match actual 3D printing conditions. Moreover, oxygen replenishment was already reduced due to the covering quartz glass.

The specific choice of materials is insignificant in demonstrating the functionality of feedback controlled photopolymerization. Arguably, even a pure photopolymer resin suffices to prove the principle for

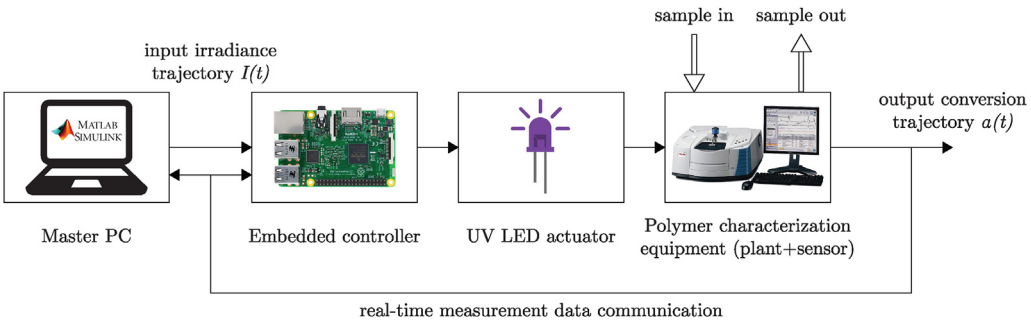

Fig. 3. Embedded control system layout. The system was obtained by augmenting existing spectrometry equipment with an actuator, an embedded controller, and an interfacing master PC.

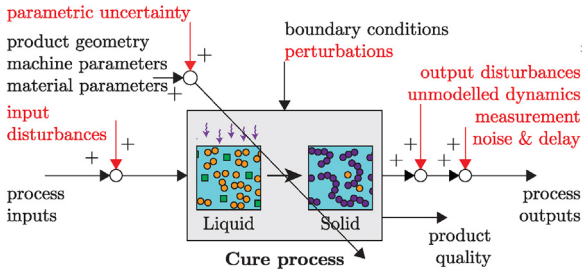

Fig. 5. Potential uncertainties (in red) in vat photopolymerization. (For interpretation of the references to colour in this figure legend, the reader is referred to the web version of this article.)

ceramic slurries, since the working principle of vat photopolymerization is exactly the same both *with* and *without* ceramic fillers. After initial tests with pure resins, an acrylate-based silica ceramic slurry (Formlabs GmbH, Berlin) was selected for this study.

2.3. Identification and application of uncertainties

Uncertainties in AM equipment, input materials, and processes ultimately lead to uncertainty in final parts [10]. Reducing sensitivity to these uncertainties is one of the main drivers behind applying feedback control. According to control theory, two types of uncertainty can be discerned [29]. On the one hand, *signal* uncertainty concerns uncertainty in the value of the input, output or measurement signals. On the other hand, *model* uncertainty concerns neglected or unmodelled dynamics and parametric uncertainty. Fig. 5 shows each of these different types of uncertainty in a block scheme of the cure process.

In this block scheme, the main *process input* variable evidently is the light intensity. The choice of the *process output* variable(s) to be used for feedback control is less evident, but the most promising output candidate seems to be the degree of conversion. This *measurable* process output can be considered merely a *secondary output*, since on a higher abstraction level the *difficult-to-measure* or *unmeasurable primary output* is product quality and the *primary input* is the product geometry and its properties. In control systems terminology, this problem can be considered an indirect or inferential control problem [13,29].

Besides input and output disturbances, potential uncertainties could be identified for each parameter and variable by developing and analyzing models of the (vat) photopolymerization process. However, the purpose of this work would be lost if this approach would be followed. Therefore, a literature screening [26,25,18] on possible error sources was performed, resulting in the following shortlist:

- Input uncertainties:
  - light source power/intensity variations;
  - light source intensity profile shape variations;
  - light source positioning errors.
- Exogenous signal uncertainties:
  - layer thickness deviations (poor recoating);
  - oxygen level fluctuations (inhibition);
  - temperature fluctuations.
- Resin parametric uncertainties:
  - deviating resin/slurry properties;
  - spatial composition variations (poor mixing).
- Unmodelled dynamics:
  - non-constant light transmission/photobleaching;
  - oversimplified reaction mechanism kinetics;
  - post-processing (cleaning) steps;
  - scattering due to ceramic particles;
  - shrinkage.

Assessing the potential performance gain that can be obtained by transitioning from open-loop to closed-loop control, would require a model of the magnitude, the occurrence probability, and the dynamics of these uncertainties. Little is known from literature about the significance of these individual uncertainties. However, the system can be subjected to intentionally applied disturbances for proof-of-principle demonstration purposes. From the uncertainties shortlist given above, it was established that it is possible to apply:

1. an artificial input disturbance by adding a signal;
2. a material composition disturbance by:
   - adding an inhibitor to the mixture;
   - pre-curing to a non-zero initial state;
   - purging with nitrogen or oxygen;
   - varying the photoinitiator concentration;
3. a thermal disturbance by cooling or heating the sample.

Among these artificial disturbances, the first is a signal uncertainty that was easily digitally applied in the control software. Therefore, initial tests were carried out with a significant input bias disturbance and these already yielded positive results. The second and third disturbances are model uncertainties that needed to be physically applied. The choice was made to add a 4-methoxyphenol inhibitor (MEHQ, Sigma-Aldrich) to the slurry, since this disturbance represents a poorly mixed or deteriorated material, which is presumably more likely to occur in the 3D printer than a significant input bias.

2.4. Experimental procedure

Since the main goal of this paper is to demonstrate the feasibility of closed-loop controlled conversion through proof-of-principle experiments, the following three situations are compared:

1. a nominal reference situation (non-disturbed);
2. a disturbed open-loop situation (controller is off);
3. a disturbed closed-loop situation (controller is on).

Fig. 6 illustrates these three situations with block schemes. First, a series of parameter identification experiments was conducted to obtain a process model relating the input $I(t)$ to the output $\alpha(t)$ under *nominal* conditions. Subsequently, the process model thus obtained was used to generate feedforward input and reference trajectories $I_{\mathrm{FF}}(t)$ and $\alpha_{\mathrm{ref}}(t)$ for use in the closed-loop control experiments under *disturbed* conditions.

Parameter identification was carried out by performing step-response experiments under *nominal* conditions, in which a step change in the input signal $I(t)$ of 5% = 1.9 W/m^2 was applied for 90 s and the change in the output $\alpha(t)$ was recorded [13]. Typically, stationary mask projection photopolymerization systems merely turn on the light source for a certain period, which in fact can be considered a step-response experiment in itself. In Section 3 a differential equation model is developed, whose analytical solution is fitted to the experimental data through least squares parameter estimation.

Open- and closed-loop control experiments were carried out under *disturbed* conditions by dissolving 0.5 wt% of inhibitor into the slurry, applying a feedforward step input $I_{\mathrm{FF}}(t)$ of 5% = 1.9 W/m^2 for 60 s, and turning the controller off or on respectively. To this end, the control schemes shown in Fig. 6 were implemented in MATLAB/Simulink.

3. Control-oriented process modelling

Many models to describe the photopolymerization process have been developed; refer to the books by Bartólo [25] and Odian [27] for a general overview of (vat) photopolymerization process modelling and a previous work by the present authors [9] for an overview of relevant phenomena and process models. However, very few models such as those reported in the works by Yebi [16] and Zhao [18] have been

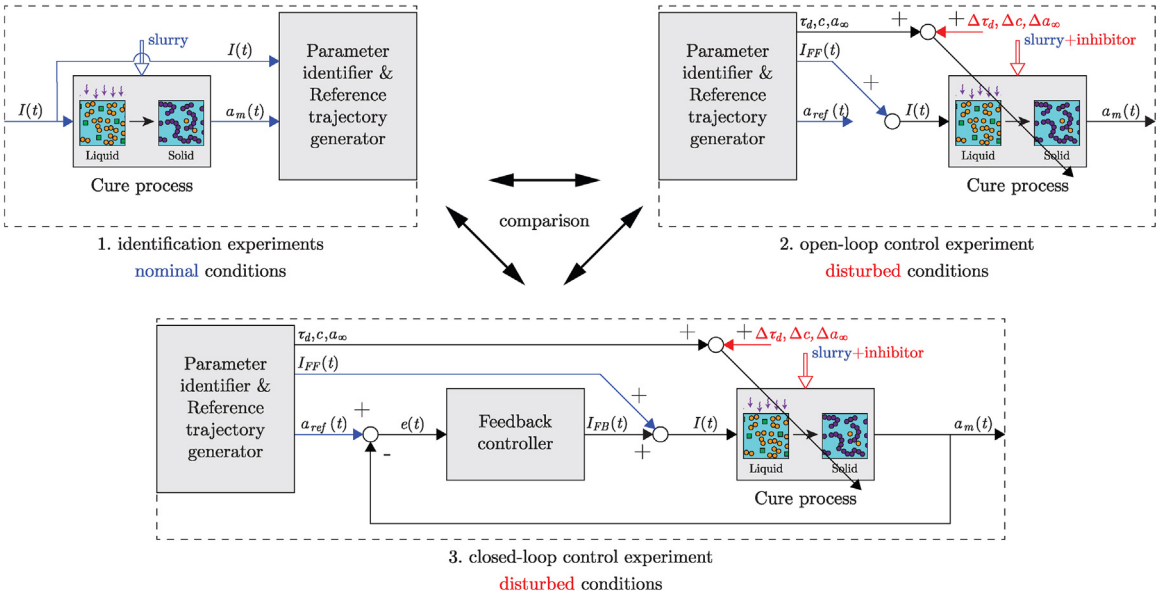

Fig. 6. Experimental procedure visualized by block schemes of the parameter identification and subsequent open- and closed-loop control experiments. The nominal conditions are indicated in blue; the material composition disturbance and consequent parametric uncertainty are indicated in red. (For interpretation of the references to colour in this figure legend, the reader is referred to the web version of this article.)

developed with the goal to use them for control purposes. Therefore, a simple, control-oriented model is developed in this section. To obtain the desired SISO model, the assumption is made that light intensity gradients in the vertical direction can be neglected within the probing volume.

3.1. Photopolymerization kinetics modelling

Two modelling approaches are typically pursued in photopolymerization kinetic modelling [25]: mechanistic or phenomenological modelling. Mechanistic models are typically set up by determining the reaction mechanisms, formulating species balances and expressions for the reaction rate constants. A typical example is the model for free radical photopolymerization by Odian [27], which is obtained by setting up species balances for the monomer, radical chains and photoinitiator, and applying a steady-state radical concentration assumption to simplify to a single differential equation:

$$\frac{d[M]}{\mathrm{dt}} = -k_p[M]\left(\frac{\phi I_a}{k_t}\right)^{1/2}, \tag{3}$$

where k_p and k_t are the propagation and termination reaction constants respectively, ϕ the quantum yield for initiation and I_a the absorbed light intensity. The degree of conversion α can be calculated by combining (3) with (2). In contrast, phenomenological models try to capture the complete polymerization reaction in one differential equation and directly compute the degree of conversion α. A typical example is given by:

$$\frac{d\alpha}{\mathrm{dt}} = k(T)I^b(1-\alpha)^n, \tag{4}$$

where $k(T)$ is the reaction rate constant as function of temperature, I is the light intensity and n is the reaction order. The exponent b can have a value between 0.5 and 1 [25], so the dependence of the polymerization rate $-\frac{d[M]}{\mathrm{dt}}$ on the input light intensity is a square-root dependence, a linear dependence or something in between. Note that for $b = 0.5$ and $n = 1$, combining (2) and (3) gives (4). Mechanistic modelling approaches often lead to models having many parameters [25], whereas phenomenological models generally result in fewer parameters and hence seem more suitable for control.

This work proposes the following control-oriented model based on the notion that photopolymerization is represented by the simple chemical reaction given by (1). Chemical kinetics theory [30] says that the rate of reaction v can be given by:

$$v = k[M]^n, \tag{5}$$

where k is the rate constant and n the reaction order. If the volume does not change during the reaction, the rate of reaction v can be replaced by the change in concentration $\frac{d[c]}{\mathrm{dt}}$ multiplied with the inverse of the stoichiometric coefficient $\frac{1}{\nu_i}$. This gives the following model:

$$\frac{d[M](t)}{\mathrm{dt}} = -k(I)[M]^n(t), \tag{6}$$

where $k(I)$ is the rate constant as function of light intensity. The rate constant is defined in the same way as in (4), but the temperature dependence is neglected:

$$k(I) = cI^b(t), \tag{7}$$

where c is a constant representative for the reaction rate. Obviously the term 'rate constant' for k from kinetics theory strictly is not correct in this case, since k is not a constant. Substituting (7) in (6) and combining with (2) gives the proposed model:

$$\frac{d[M](t)}{\mathrm{dt}} = -\mathrm{c}I^b(t)[M]^n(t), \tag{8}$$

$$\alpha(t) = 1 - \frac{[M](t)}{[M]_0}, \tag{9}$$

with the initial condition $[M](0) = [M]_0$ and the physical constraint that energy can only be added by irradiation:

$$I(t) \geq 0. \tag{10}$$

Eq. (3) is retrieved for $b = 0.5$ and by taking $k(I) = k_p\sqrt{\frac{\phi I}{k_t}}$. Another physical constraint is that the monomer concentration $[M]$ is non-negative.

In control systems terminology, the *input* variable $u(t)$ to the system is the light intensity $I(t)$, the internal *state* variable $x(t)$ is the monomer concentration $[M](t)$, and the *output* variable $y(t)$ is the degree of conversion $\alpha(t)$. Using these naming conventions, the model can be rewritten as a state and output equation:

$$\frac{\mathrm{d}x(t)}{\mathrm{d}t} = -c \cdot u^b(t) \cdot x^n(t), \tag{11}$$

$$y(t) = 1 - \frac{x(t)}{x_0}, \tag{12}$$

with the initial condition $x(0) = x_0$ and the input constraint:

$$u(t) \geq 0. \tag{13}$$

Note that (11) and (12) can also be combined to a single ordinary differential equation in terms of y by eliminating x. The model (3) suggests a first-order reaction, but second-order reactions are reported in literature as well [27], so $n \in \{1, 2\}$ is considered in this paper. Note that the *reaction order* in chemical kinetics is different from the *system order* in control systems theory; the former refers to the sum of the exponents n of the reaction rate, whereas the latter refers to the number of states, i.e., the dimension of the state vector $x(t)$, which in this case is one.

3.2. Analytical solutions for parameter estimation

The ordinary differential equations (8) and (11) have analytical solutions for a constant input light intensity $I(t)$ and a given reaction order n, which can be used to write explicit solutions for the conversion $\alpha(t)$. The existence of these solutions is the reason to use step-response experiments for parameter identification. In these experiments, the following input $u_{\mathrm{FF}}(t)$ is applied:

$$u_{\mathrm{FF}}(t) = \begin{cases} 0, & t < t_{\mathrm{step}} \\ I_{\mathrm{step}}, & t_{\mathrm{step}} \leq t < t_{\mathrm{end}} \\ 0, & t \geq t_{\mathrm{end}} \end{cases} \tag{14}$$

where t_{step} is the instant the light turns on, t_{end} the instant the light turns off, and I_{step} is the feedforward intensity.

The first step-response experiments showed a noticeable delay between the instant the light was turned on and the instant the process started to respond. This time-delay behaviour is well known for free radical photopolymerization [26,31] and is attributable to the consumption of inhibitors before the chain reaction can rapidly speed up. This high-order system behaviour can be approximated with a pure time delay in the input [13]. To model this behaviour, the feedforward input (14) is delayed by τ_d such that $u_{\mathrm{FF},d}(t) = u_{\mathrm{FF}}(t - \tau_d)$ and set to zero once the light is turned off at t_{end}:

$$u_{\mathrm{FF},d}(t) = \begin{cases} 0, & t < t_{\mathrm{step}} + \tau_d \\ I_{\mathrm{step}}, & t_{\mathrm{step}} + \tau_d \leq t < t_{\mathrm{end}} \\ 0, & t \geq t_{\mathrm{end}}. \end{cases} \tag{15}$$

Note that this time-delayed feedforward input $u_{\mathrm{FF},d}(t)$ is only applied in simulations with the model (8) or (11), whereas the non-delayed input $u_{\mathrm{FF}}(t)$ is applied in physical experiments.

The analytical solution to (8) with the input (15) for a first-order reaction, i.e., $n = 1$, is well known [13] and using this solution with (9) gives:

$$\alpha(t) = \begin{cases} 0, & t < t_{\mathrm{step}} + \tau_d \\ 1 - e^{-\mathrm{cI}_{\mathrm{step}}^b (t - (t_{\mathrm{step}} + \tau_d))}, & t_{\mathrm{step}} + \tau_d \leq t < t_{\mathrm{end}} \\ \alpha_{\mathrm{end}}, & t \geq t_{\mathrm{end}}, \end{cases} \tag{16}$$

where τ_d is a time delay and $\alpha_{\mathrm{end}} = 1 - e^{-\mathrm{cI}_{\mathrm{step}}^b (t_{\mathrm{end}} - (t_{\mathrm{step}} + \tau_d))}$. In control systems terminology, this is the solution for a first-order system with time delay [13].

Similarly, the analytical solution to (8) with the input (15) for a second-order reaction, i.e., $n = 2$, can be derived and using this solution with (9) gives:

$$\alpha(t) = \begin{cases} 0, & t < t_{\mathrm{step}} + \tau_d \\ 1 - \dfrac{1}{1 + [M]_0 \mathrm{cI}_{\mathrm{step}}^b (t - (t_{\mathrm{step}} + \tau_d))}, & t_{\mathrm{step}} + \tau_d \leq t < t_{\mathrm{end}} \\ \alpha_{\mathrm{end}}, & t \geq t_{\mathrm{end}} \end{cases} \tag{17}$$

where $\alpha_{\mathrm{end}} = 1 - \frac{1}{1 + [M]_0 \mathrm{cI}_{\mathrm{step}}^b (t_{\mathrm{end}} - (t_{\mathrm{step}} + \tau_d))}$.

The model (8), (9) assumes that all monomer M can be converted into polymer, which implies that $\alpha \in [0, 1]$. However, in practice the degree of conversion reaches an asymptote $\alpha_\infty < 1$ [4], so the degree of conversion as defined by (9) and the analytical solutions (16) and (17) should be considered a normalized degree of conversion. The measured absolute degree of conversion α_m can be obtained by introducing a degree of conversion asymptote α_∞:

$$\alpha_m(t) = \alpha_\infty \alpha(t). \tag{18}$$

3.3. Sensor modelling

The FTIR spectrometer does not directly output the desired degree of conversion $\alpha_m(t)$ sensor signal, so post-processing is required to compute $\alpha_m(t)$ from the absorbance spectra $A(\tilde{\nu}, t_i)$ as function of the wavenumber $\tilde{\nu} \in [400, 4000]\,\mathrm{cm}^{-1}$ and time instance t_i. A typical way to do this is to calculate the baseline-corrected areas under the reference peak A_{ref} and the carbon-carbon double bond C═C peak A_{CC} [32,33]. This way, the peak area ratio $r_{\mathrm{pA}}(t)$ can be calculated:

$$r_{\mathrm{pA}}(t) = \frac{A_{C=C}(t)}{A_{\mathrm{ref}}(t)}. \tag{19}$$

The degree of conversion can be computed from (19) by dividing it by the initial peak area ratio $r_{\mathrm{pA},0}$ [33]:

$$\alpha_m(t) = 1 - \frac{r_{\mathrm{pA}}(t)}{r_{\mathrm{pA},0}}, \quad t > 20\,\mathrm{s}, \tag{20}$$

where $r_{\mathrm{pA},0}$ was determined by averaging $r_{\mathrm{pA}}(t)$ in the range $t \in [0, 20]\,\mathrm{s}$. This initialization time was chosen such that ten samples were used to calculate $r_{\mathrm{pA},0}$, each having a sampling time $T_s = 2.0\,\mathrm{s}$. Note that the degree of conversion was only available online after the 20 s initialization period.

IR absorbance spectra of the Formlabs silica material showed that a practically constant peak in the $1750\,\mathrm{cm}^{-1}$ region could be used as the reference peak, which is associated to C═O stretching [32]. Moreover, the spectra showed that the peak $A_{C=C}$ in the $1635\,\mathrm{cm}^{-1}$ region could be used to quantify the carbon-carbon double bond (C═C) or monomer concentration $[M]$.

3.4. Feedback controller design

A first step in the feedback controller design process is to choose the type of controller to be used. A choice could best be made based on the specific *control problem* at hand. To this end, one could attempt to classify the control problem according to characteristics such as the degree of nonlinearity and the dynamic character of the process behaviour [13]. The control-oriented model given by (11) and (12) can be classified as a low-order nonlinear SISO system that is either linear ($b = 1$) or nonlinear ($b \neq 1$) in the input with input constraints. If the reaction order $n = 1$ and $b = 1$, the system is termed a *bilinear* system [34,35]; if $n = 2$ the system belongs to a class of nonlinear systems that may be feedback linearizable [36]. It can be concluded that the system dynamics at hand are simple, but nonlinear.

The nonlinear system dynamics suggest that a special-purpose controller may be more effective than a classical controller. The control schemes previously developed by Yebi et al. [14–16] can be considered more advanced than classical, but cannot be applied here due to the difference in control objectives and due to the spatially-distributed (1D) and multi-layer nature of their control problem. Moreover, the goal of

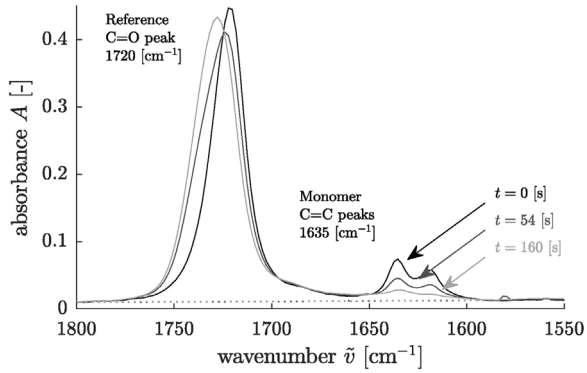

Fig. 7. IR absorbance spectrum of the Formlabs silica slurry at three different times upon UV curing. The baselines and division line between the peaks are indicated by the dotted lines. Over the course of the cure process, the baseline-corrected reference peak (175 cm^{-1} region) remains constant and the C=C peak (1635 cm^{-1} region) decreases.

this work is not to optimize a feedback controller for stability and performance, but to demonstrate disturbance rejection through a proof-of-principle experiment. Thus, a logical starting point is the most commonly used classical feedback controller: the proportional-integral-derivative (PID) controller [37,13], which was also proposed by Zhao and Rosen as a substitute to their simple binary on-off controller [21,18]. Moreover, classical control strategies serve as a benchmark for more advanced control strategies. Due to the rather noisy output signal, the choice was made to omit the derivative action and use a proportional-integral (PI) controller to prevent noise amplification.

A PI controller typically has the form [13,37]:

$$u_{\mathrm{FB}}(t) = K_c\left[e(t) + \frac{1}{\tau_I}\int_0^t e(t)\mathrm{dt}\right], \tag{21}$$

where K_c is the *proportional* gain, $e(t)$ the error, and τ_I the *integral* time. The error signal is defined as the difference between the reference $r(t) = \alpha_{\mathrm{ref}}(t)$ and the measured output $y(t) = \alpha_m(t)$:

$$e(t) = \alpha_{\mathrm{ref}}(t) - \alpha_m(t). \tag{22}$$

Referring to Fig. 6, the *input* to the PI controller is the error $e(t)$ and the *output* from the controller is the light intensity $u_{\mathrm{FB}}(t) = I_{\mathrm{FB}}(t)$. Consequently, the total light intensity $I(t)$ applied to the cure process equals the sum of (14) and (21):

$$I(t) = I_{\mathrm{FF}}(t) + I_{\mathrm{FB}}(t). \tag{23}$$

The working principle of the PI controller can be interpreted as follows. If there is a positive error $e(t)$ between the reference $\alpha_{\mathrm{ref}}(t)$ and the actual output conversion $\alpha_m(t)$, i.e., the cure process is not quick enough, then the proportional action of the controller will apply a positive feedback input $u_{\mathrm{FB}}(t)$ to increase the reaction rate and vice versa if there is a negative error the proportional action will apply a negative feedback. Additionally, if the time integral of the error $e(t)$ is positive even if the error is momentarily small, the integral action will increase the reaction rate and vice versa decrease if the time integral is negative.

After choosing the PI controller type, the next step was to find suitable controller parameters K_c and τ_I. To this end, a common controller tuning approach based on an approximate model was applied [13]. The approach consists of fitting an approximate model to the process reaction curve $y(t)$ and using the obtained parameters in specific formulas that give recommended controller parameter values. The most commonly applied approximate model is a first-order system with time delay of the form:

$$\tau\frac{\mathrm{dy}(t)}{\mathrm{dt}} = -y(t) + \mathrm{K}\,\mathrm{u}(t-\tau_d), \tag{24}$$

where τ is the effective time constant, K the steady-state gain, and τ_d the effective time delay. The response $y(t)$ of the first-order system (24) to a step input $u(t)$ is equal to the response of the first-order reaction (16) with $\tau = (\mathrm{cI}_{\mathrm{step}}^{b})^{-1}$. Note that although the process responses are equal, the underlying system dynamics differ from each other. Having fit the approximate model to the process response, the controller parameters were obtained from the Integral Time-weighted Absolute Error (ITAE) tuning rule for set-point changes [13]:

$$K_c = \frac{0.586}{K}\left(\frac{\tau}{\tau_d}\right)^{0.916}, \qquad \tau_I = \frac{\tau}{1.03 - 0.165\left(\frac{\tau_d}{\tau}\right)}. \tag{25}$$

4. Results

4.1. Parameter identification under nominal conditions

Step response experiments were performed by applying a step input, recording the absorbance spectra, and computing the degree of conversion. Fig. 7 shows the resulting time evolution of the IR absorbance spectrum in the spectral range of interest. As expected, the figure shows that the baseline-corrected area remains practically constant under the reference C=O peak in the 1750 cm^{-1} region, whereas the area decreases significantly under the C=C peaks in the 1635 cm^{-1} region.

From these absorbance spectra, the ratio r_{pA} was computed between the double bond and reference peak areas to determine the degree of conversion $\alpha_m(t)$. Fig. 8 shows the time evolution of the peak area ratio $r_{\mathrm{pA}}(t)$ and the estimated initial peak area ratio $r_{\mathrm{pA},0}$. The figure shows a steep decrease in the peak area ratio approximately 12 s *after* the light had been turned on. To determine the conversion *online*, the initial peak area ratio was determined *before* the light was turned on. This functionality was implemented in the Simulink control scheme by taking the average of the peak area ratios between $t = 0$ s and $t = 20$ s and storing in memory for the remainder of the experiment.

Once the initial peak area ratio had been determined, the degree of conversion was computed at each time step and made available for real-time feedback control. A typical resulting degree of conversion measurement is shown in Fig. 9 along with first- and second-order reaction model fits. Among the two, only the second-order reaction model shows an acceptable fit for the intended purpose, so the model parameter $n = 2$ for this material.

This model fitting procedure was performed for ten equally spaced input levels I_{step} from 10% to 100% and an additional level at 5% with three replications per level in a randomized sequence. Fig. 10 shows the

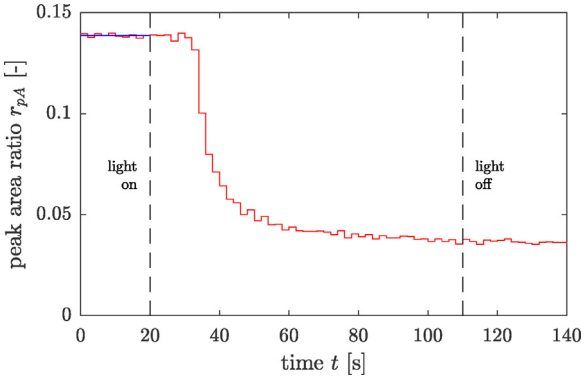

Fig. 8. Peak area ratio of the Formlabs silica slurry during UV curing. The samples between 0 and 20 s are used to determine the initial peak area ratio (blue). Twelve seconds after irradiation starts, the response shows a steep decrease. (For interpretation of the references to colour in this figure legend, the reader is referred to the web version of this article.)

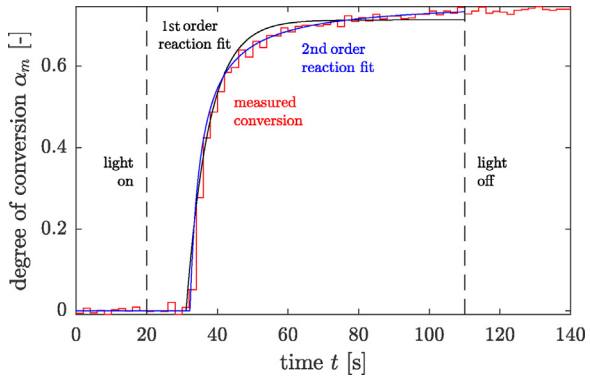

Fig. 9. Degree of conversion determined from IR absorbance spectra during UV curing. First- and second-order reaction model fits were fitted to the experimental data; the second-order reaction model shows an acceptable goodness of fit.

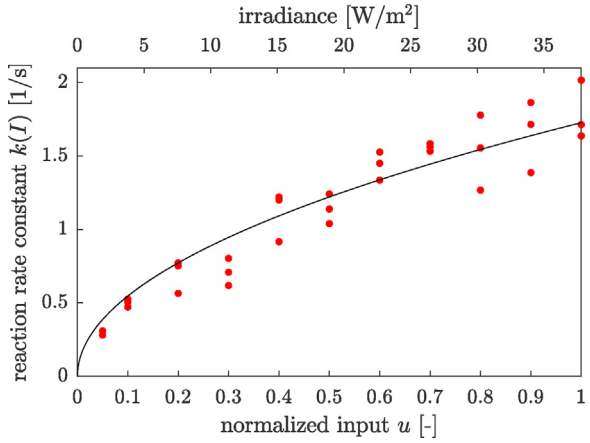

Fig. 10. Identified reaction rates k as a function of light intensity I. Results conform to the well-known square-root dependency, whose fit to the experimental data is given by the solid line.

resulting identified reaction rate k as a function of normalized light intensity I, along with a square root function fit. The experimental data is in accordance with the well-known square-root dependency [27], so the model parameter $b = 0.5$ for this material. Note that the higher the input, the closer the time constant $\tau = \frac{e-1}{k(I)}$ approaches the temporal resolution or sampling time T_s, which may explain the seemingly increasing variance with intensity.

To approximate the variance at a single level, a repeatability experiment was performed with ten replications at $I_{\text{step}} = 5\%$. Table 1 shows the parameters identified from this data and their respective standard deviations. The second-order reaction model was fully parameterized at this point and was subsequently used to generate a nominal reference trajectory $\alpha_{\text{ref}}(t)$ to be followed by the output $\alpha_m(t)$.

4.2. Open- and closed-loop control under disturbed conditions

Once the parameter identification procedure under *nominal, non-disturbed* conditions had been completed, the open- and closed-loop control experiments were performed under *disturbed* conditions. Firstly, the controller parameters were obtained by filling in the identified first-order model parameters in the tuning rule (25). Table 2 gives the resulting model and controller parameters. Secondly, the silica slurry *with* inhibitor was used and the feedback controller was either turned off or on. Figs. 11 and 12 show the measured degree of conversion $\alpha_m(t)$ and the inputs $u(t)$ respectively for the three different cases: (1) the non-disturbed reference situation, (2) the disturbed open-loop situation, and (3) the disturbed closed-loop situation.

Table 1
Summary of identified model parameter means ± standard deviations.

Resin	b	n	c [s^{-1}]	τ_d [s]	α_∞
Formlabs silica	0.5	2	1.3 ± 0.2	12 ± 0.6	0.77 ± 0.01

Table 2
First-order approximate model and PI controller parameters.

Parameter	K	τ [s]	τ_d [s]	K_c	τ_I [s]
Value	13.9	3.44	2	0.069	3.68

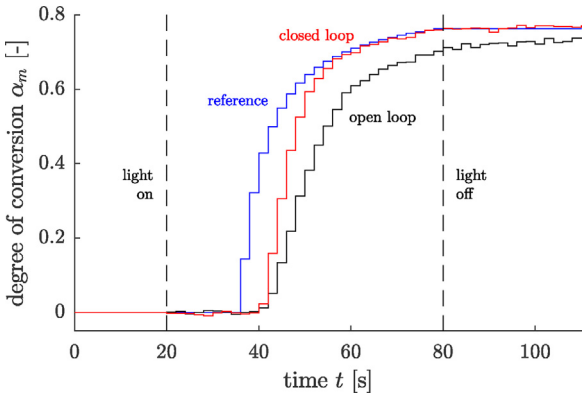

Fig. 11. Degree of conversion vs. time for the reference, open-, and closed-loop controlled case. The open-loop case shows a reduced level of curing with respect to the reference. On the contrary, the closed-loop case meets the desired final conversion level.

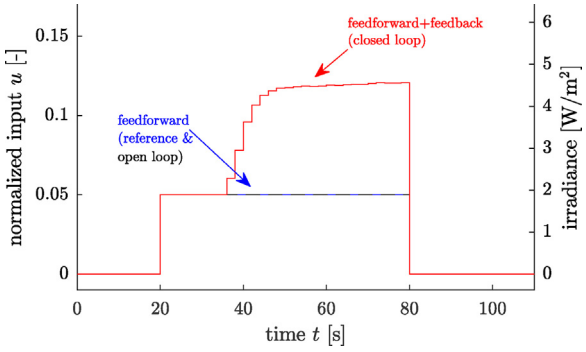

Fig. 12. Total input vs. time for the reference, open-, and closed-loop controlled case. The closed-loop case shows significant corrective action to compensate for the presence of inhibitor in the slurry.

Comparing the open-loop case with the reference case, the open-loop response in Fig. 11 shows an increasing error over time with respect to the reference. On the contrary, the closed-loop case shows that the feedback controller attempts to minimize this error through significant corrective action as evident from Fig. 12. If the final reference conversion value is considered a minimal threshold for sufficient curing, then it is *not* met in the open-loop case, but it *is* in the closed-loop case. Hence the material composition disturbance is successfully compensated for and the principle of real-time feedback control is proven in this experimental setting.

5. Discussion

The experimental results in Section 4 clearly demonstrate that a feedback controller was successful in compensating for an intentionally applied material disturbance in a dedicated lab setup. Notwithstanding

these promising results, several comments have to be made regarding the experimental results and the limitations of the present experimental setup. The sensing requirements also need to be revisited to draw conclusions on the feasibility of the in-situ real-time control approach in a large-scale machine setting.

5.1. Parameter identification experiments

The lab-scale identification experiments in Fig. 9 show that the second-order reaction model provides a good fit, since the error falls within the measured signal's noise level. Although effective for the majority of the polymerization reaction, the control-oriented model is not capable of accurately describing the reaction kinetics during the initial inhibition period or the final dark polymerization period. Many physical phenomena were excluded from this (over-)simplified model, such as spatial variations due to light absorption, photoinitiator depletion, oxygen inhibition, and heat and mass transfer [9]. Nevertheless, the second-order reaction model is considered acceptable for the purpose of this paper since it is merely used to generate the reference trajectory for the feedback control experiments.

The results also show a rather significant variability in the identified reaction rate constant and time delay. This parameter variability can be considered representative of the total process variability, which is affected by uncertainties in the actuator, the sensor, the data processing and communication, the embedded controller, and the photopolymer itself. However, it is difficult to draw conclusions on how much each source of variability contributes to the total variability and to what extent these uncertainties are encountered in real-life industrial AM machines. In the setup, significant variability may result from the manual deposition of material and the free support of the covering glass on the spacer. These factors may lead to layer thickness deviations and hence to reaction rate variability due to light intensity variations when one assumes Beer–Lambert-like absorption [27].

5.2. Control experiments

The ultimate control objective is to reduce variability in final product quality and compensate for disturbances, but product quality is not easily or directly measurable. Firstly, product quality needs to be defined and quantified by metrics [11]. Secondly, the difficulty of measurability implies that product quality needs to be inferred from measurable quantities such as the degree of conversion. Therefore, the question arises what the relationship is between the degree of conversion and the mechanical properties, which ultimately express product quality. Moreover, the question arises what shape the reference conversion trajectory $\alpha_{\text{ref}}(t)$ should have such that the desired mechanical properties are obtained. To the author's knowledge, it is still an open research question whether the complete time evolution of the reaction $\alpha_{\text{ref}}(t)$ should be closely tracked, or merely the final degree of conversion value $\alpha(t_{\text{end}})$ should be met.

Recent literature reports significant sensitivity of mechanical properties to differences in conversion levels [24,38,39]. This sensitivity implies that if the final reference conversion value is considered a minimal threshold, then the open-loop controlled case in Fig. 11 would have led to product defects in contrast to the closed-loop case. In other words, the closed-loop case clearly outperforms the open-loop case. However, the opportunities and benefits are yet to be explored in terms of implementing the closed-loop controller in a real AM machine. The material composition disturbance applied in the experiment was for demonstration purposes of the closed-loop control principle, and not intended to be representative for the typical disturbances encountered in an industrial AM setting.

Further performance improvements may be gained by exploiting the potentially fast actuation capabilities of UV light. This work merely applies a constant feedforward step input, which actually is representative for the curing of a single layer in digital mask projection systems. Note that the point of interest at the bottom of the layer receives multiple step inputs of decreasing intensity from successive layers. Different input profiles during the curing of each layer may yield better mechanical properties such as the initially lower intensities in soft-start photopolymerization [40].

5.3. Limitations of the experimental setup

A persistent issue faced by researchers is that light intensities need to be reduced to match the reaction and measurement timescales in in-situ photopolymer characterization [41]. Moreover, the achievable control system performance is heavily influenced by the sensor's measurement rate, which is rather limited in the present setup. Particularly, a key metric for achievable control system performance is the ratio of the process dynamics time constant to the sampling time: $\frac{\tau}{T_s}$. In the system at hand, the reaction time constant is inversely proportional to the nominal light intensity $\tau \propto I_{\text{FF}}^{-1}$.

An acceptable ratio $\frac{\tau}{T_s}$ was achieved by choosing a sufficiently low nominal input intensity, which is consistent with common practice [41]. The hence achieved measurement time was $T_s = 2.0$ s. This rather low value was due to (1) the FTIR spectrometer settings and (2) the overhead in the self-developed software interface between the FTIR spectrometer and MATLAB/Simulink. Note that the spectrometer was not designed for real-time control experiments and hence did not natively support real-time data output.

As a result of the low nominal light intensity, the achieved reaction rate time constant $\tau = 8$ s and exposure time of $t_{\text{exp}} = 60$ s are much larger than in typical mask projection systems, where exposure times range from 1 to 10 s per layer. Options to increase the sampling rate are under investigation to allow for increased UV light intensities and, hence, a closer match to actual printing conditions.

5.4. Implications of the control approach in a large-scale machine setting

Several steps have to be taken before the present work's real-time control approach can be implemented in real, large-scale AM machines. Fig. 13 suggests a sequence of steps from 0D sub-voxel control as demonstrated in this work to full 3D product control. Firstly, the vertical dimension needs to be considered to scale up to a single homogeneous layer or 1D voxel. Therefore, a 1D *depth-resolved* degree of conversion measurement $\alpha(z)$ or a *layer-averaged* degree of conversion value $\bar{\alpha}$ needs to be available, as opposed to a 0D point measurement.

Secondly, the lateral dimensions need to be considered to scale up to a 2D array of 1D voxels in the xy-plane. Implementation of the present control approach in a real AM machine is most easily envisioned in stationary digital mask projection systems, where each pixel of the projection system is associated to a surface voxel as depicted in Fig. 2. Zhao and Rosen have already shown that scaling up laterally in mask projection systems is a matter of using an array detector [17]. In the most simple case, the closed-loop control system presented here can be implemented as multiple parallel SISO systems. Each surface voxel can then be considered a SISO system having its own boundary light intensity input modulated by the projector system, its own layer-averaged degree of conversion measurement, and its own feedback controller. In a more involved case, a multiple-input-multiple-output (MIMO) control strategy could be implemented to address cross-talk between neighbouring pixels.

Thirdly, the single-layer scope needs to be extended to multiple layers. In the most simple case, the single-layer controller in this paper could be reset for each new layer, without considering the effect of UV exposure of the current layer on previously cured layers. Alternatively, the exposure of a layer to subsequent doses can be compensated for in the process planning phase when determining the feedforward step input. More performance may be gained by utilizing a 3D full-field measurement $\alpha(x, y, z)$ of the degree of conversion and applying

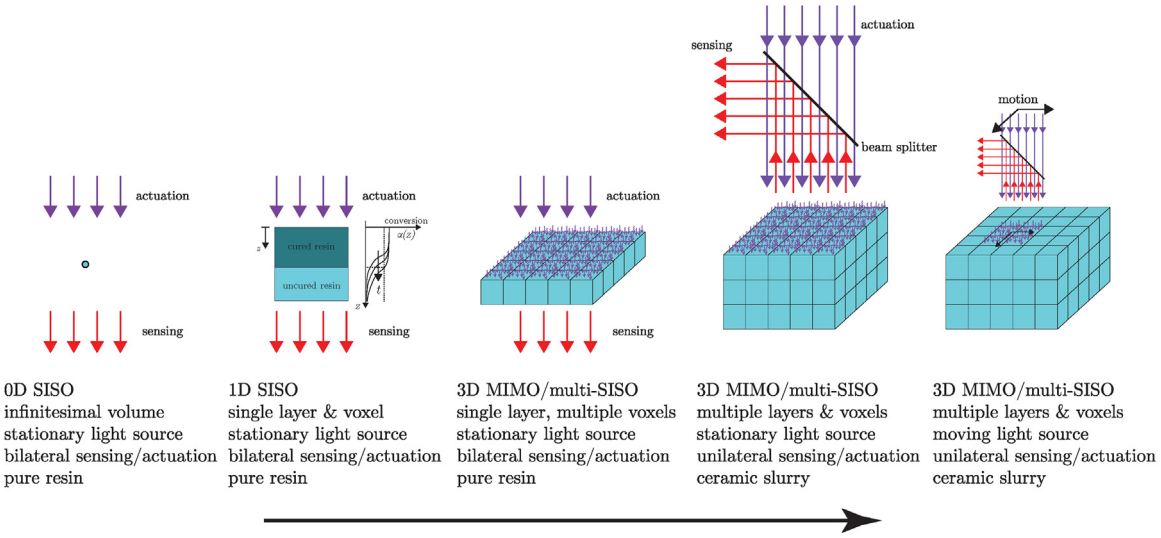

Fig. 13. Proposed roadmap from single 0D sub-voxel control to full 3D product control.

model-based control techniques such as those by Yebi et al. [14]. Additionally, multi-level control architectures can be envisioned where real-time in-situ continuous control is combined with discrete layer-to-layer or product control [22]. However, even though the control problem can be extended to a full 3D field, the UV light input remains a 2D input field at the boundary (surface) of the layer.

Lastly, light sources moving in the xy-plane need to be addressed to enable implementation of the real-time control approach in vector scanning or scanning mask projection systems [42]. Control strategies for metal-based processes such as melt-pool area or temperature control [11] may be applied to the analogous control problem for photopolymerization-based processes.

The aforementioned scaling-up procedure requires a 3D full-field degree of conversion sensor, having a high spatio-temporal resolution, a range spanning a considerable build volume, and being capable of measuring and actuating on the same side, e.g., in a reflective mode. Such a sensor is not yet available and the feasibility of implementing an FTIR spectrometer into the vat photopolymerization machine is arguable. Light scattering due to the presence of ceramic particles in the resin [4,43] may further complicate the applicability of such optical cure monitoring techniques. However, the presented control approach will also work for other measuring technologies, as long as they provide representative sensing signals for the degree of cure. Moreover, plans have been reported of implementing a Raman spectrometer into a vat photopolymerization machine [44]. If real-time degree of cure sensing for continuous control ultimately proves to be impractical in the AM machine, alternative discrete control strategies [22] may be considered. For instance, an in-situ calibration method can be conceived that determines the key material properties offline, but in the machine through parameter identification techniques such as those presented in this work rather than current tedious working curve procedures [26,45].

6. Conclusions

This work demonstrated closed-loop control feasibility of monomer conversion in (ceramic) vat photopolymerization through proof-of-principle experiments. The experiments showed that a feedback controller was successful in compensating for a material perturbation in a small-scale setup. Moreover, a simple control-oriented process model proved to be well capable of describing the photopolymerization system behaviour under lab conditions. These promising results can be considered a fundamental step towards real-time in-situ control of the polymerization reaction that lies at the core of vat photopolymerization technology. Ultimately, such in-line process control strategies are expected to play a key role in the industrialization of vat photopolymerization based AM, as well as in other AM technologies.

Acknowledgements

This study was funded by the Netherlands Organisation for Applied Scientific Research (TNO) and was carried out within the AMSYSTEMS Center. The authors would like to thank their colleagues from the TNO Materials Sciences department for their support and use of FTIR spectrometry equipment.

References

[1] I. Gibson, D. Rosen, B. Stucker, Additive Manufacturing Technologies, 2nd edition, Springer, New York, NY, 2015, https://doi.org/10.1007/978-1-4939-2113-3.
[2] A. Zocca, P. Colombo, C.M. Gomes, J. Günster, Additive manufacturing of ceramics: issues, potentialities, and opportunities, J. Am. Ceram. Soc. 98 (7) (2015) 1983–2001, https://doi.org/10.1111/jace.13700.
[3] T. Chartier, Additive manufacturing to produce complex 3D ceramic parts, J. Ceram. Sci. Technol. 6 (2) (2015) 95–104, https://doi.org/10.4416/JCST2014-00040.
[4] J.W. Halloran, Ceramic stereolithography: additive manufacturing for ceramics by photopolymerization, Annu. Rev. Mater. Res. 46 (1) (2016) 19–40, https://doi.org/10.1146/annurev-matsci-070115-031841.
[5] T. Ohji, Additive manufacturing of ceramic components, Synthesiology 11 (2) (2018) 81–93, https://doi.org/10.5571/synth.11.2_81.
[6] S.C. Ligon, R. Liska, J. Stampfl, M. Gurr, R. Mülhaupt, Polymers for 3D printing and customized additive manufacturing, Chem. Rev. 117 (15) (2017) 10212–10290, https://doi.org/10.1021/acs.chemrev.7b00074.
[7] P. Colombo, G. Mera, R. Riedel, G.D. Sorarú, Polymer-derived ceramics: 40 years of research and innovation in advanced ceramics, J. Am. Ceram. Soc. 93 (7) (2010) 1805–1837, https://doi.org/10.1111/j.1551-2916.2010.03876.x.
[8] T. Hafkamp, G. van Baars, B. de Jager, P. Etman, A trade-off analysis of recoating methods for vat photopolymerization of ceramics, Proceedings Solid Freeform Fabrication Symposium (2017) 687–711.
[9] T. Hafkamp, G. van Baars, B. de Jager, P. Etman, A feasibility study on process monitoring and control in vat photopolymerization of ceramics, Mechatronics 56 (2018) 220–241, https://doi.org/10.1016/j.mechatronics.2018.02.006.
[10] J. Pellegrino, T. Makila, S. McQueen, E. Taylor, Measurement science roadmap for polymer-based additive manufacturing, Tech. Rep. NIST AMS 100-5, National Institute of Standards and Technology, Gaithersburg, MD, December 2016http://nvlpubs.nist.gov/nistpubs/ams/NIST.AMS.100-5.pdf.
[11] M. Mani, B. Lane, A. Donmez, S. Feng, S. Moylan, R. Fesperman, Measurement science needs for real-time control of additive manufacturing powder bed fusion processes, Tech. Rep. NIST IR 8036, National Institute of Standards and Technology, February 2015, http://nvlpubs.nist.gov/nistpubs/ir/2015/NIST.IR.8036.pdf.
[12] W.F. Reed, A.M. Alb (Eds.), Monitoring Polymerization Reactions: From Fundamentals to Applications, John Wiley & Sons, Inc., Hoboken, NJ, 2014.
[13] B.A. Ogunnaike, W.H. Ray, Process Dynamics, Modeling, and Control, Topics in Chemical Engineering, Oxford University Press, New York, 1994.
[14] A. Yebi, B. Ayalew, Hybrid modeling and robust control for layer-by-layer manufacturing processes, IEEE Trans. Control Syst. Technol. 25 (2) (2017) 550–562,

https://doi.org/10.1109/TCST.2016.2558626.
[15] A. Yebi, B. Ayalew, S. Pilla, X. Yu, Model-based robust optimal control for layer-by-layer ultraviolet processing of composite laminates, J. Dyn. Syst. Meas. Control 139 (2) (2016), https://doi.org/10.1115/1.4034782 021008-1–021008-11.
[16] A.M. Yebi, Model-based control of UV curing processes with application to additive manufacturing (Ph.D. thesis), Clemson University, Clemson, SC, 2015http://gradworks.umi.com/37/22/3722489.html.
[17] X. Zhao, D.W. Rosen, An implementation of real-time feedback control of cured part height in Exposure Controlled Projection Lithography with in-situ interferometric measurement feedback, Addit. Manuf. 23 (2018) 253–263, https://doi.org/10.1016/j.addma.2018.07.016.
[18] X. Zhao, Process measurement and control for exposure controlled projection lithography (Ph.D. thesis), Georgia Institute of Technology, 2017, https://smartech.gatech.edu/handle/1853/58294.
[19] R. Schwalm, UV Coatings Basics, Recent Developments and New Applications, Elsevier, Amsterdam; London, 2007http://site.ebrary.com/id/10155873.
[20] J. Steinhaus, B. Hausnerova, T. Haenel, M. Großgarten, B. Möginger, Curing kinetics of visible light curing dental resin composites investigated by dielectric analysis (DEA), Dent. Mater. 30 (3) (2014) 372–380, https://doi.org/10.1016/j.dental.2013.12.013.
[21] X. Zhao, D.W. Rosen, Investigation of advanced process control methods for exposure controlled projection lithography, Solid Freeform Fabrication Symposium Proceedings (2014) 143–162 http://sffsymposium.engr.utexas.edu/sites/default/files/2014-014-Zhao.pdf.
[22] T. Hafkamp, G. van Baars, B. de Jager, P. Etman, A classification scheme for AM control strategies: the AM V-model, Proceedings of the 2018 ASPE and euspen Summer Topical Meeting – Advancing Precision in Additive Manufacturing, vol. 69 (2018) 161–166.
[23] G.E. Fonseca, M.A. Dubé, A. Penlidis, A critical overview of sensors for monitoring polymerizations, Macromol. React. Eng. 3 (7) (2009) 327–373, https://doi.org/10.1002/mren.200900024.
[24] J. Wu, Z. Zhao, C.M. Hamel, X. Mu, X. Kuang, Z. Guo, H.J. Qi, Evolution of material properties during free radical photopolymerization, J. Mech. Phys. Solids 112 (2018) 25–49, https://doi.org/10.1016/j.jmps.2017.11.018.
[25] P.J. Bartolo (Ed.), Stereolithography, Springer US, Boston, MA, 2011, , https://doi.org/10.1007/978-0-387-92904-0.
[26] P. Jacobs, Rapid Prototyping & Manufacturing: Fundamentals of Stereolithography, Society of Manufacturing Engineers, Dearborn, MI, 1992.
[27] G.G. Odian, Principles of Polymerization, 4th edition, Wiley-Interscience, Hoboken, NJ, 2004.
[28] Y. Tang, Stereolithography cure process modeling (Ph.D. thesis), Georgia Institute of Technology, Atlanta, GA, 2005https://smartech.gatech.edu/handle/1853/7235.
[29] S. Skogestad, I. Postlethwaite, Multivariable Feedback Control: Analysis and Design, 2nd edition, Wiley, New York, 2005.
[30] K.J. Laidler, Chemical Kinetics, 3rd edition, HarperCollins, New York, 1987.
[31] Y. Brulle, A. Bouchy, B. Valance, J.C. André, Industrial photochemistry. XXI. Chemical, transport and refractive index effects in space-resolved laser photopolymerization, J. Photochem. Photobiol. A: Chem. 83 (1) (1994) 29–37 http://www.sciencedirect.com/science/article/pii/1010603094030839.
[32] K.C. Wu, J.W. Halloran, Photopolymerization monitoring of ceramic stereolithography resins by FTIR methods, J. Mater. Sci. 40 (1) (2005) 71–76, https://doi.org/10.1007/s10853-005-5689-y.
[33] X. Fernàndez-Francos, S.G. Kazarian, X. Ramis, À. Serra, Simultaneous monitoring of curing shrinkage and degree of cure of thermosets by attenuated total reflection Fourier transform infrared (ATR FT-IR) spectroscopy, Appl. Spectrosc. 67 (12) (2013) 1427–1436, https://doi.org/10.1366/13-07169.
[34] R.R. Mohler, Bilinear Control Processes: With Applications to Engineering, Ecology, and Medicine, No. 106 in Mathematics in Science and Engineering, Academic Press, New York, 1973.
[35] D.L. Elliott, Bilinear Control Systems: Matrices in Action, No. 169 in Applied Mathematical Sciences, Springer, Dordrecht, 2009.
[36] H.K. Khalil, Nonlinear Systems, 3rd edition, Prentice Hall, New Jersey, 2002.
[37] W.S. Levine, Control System Fundamentals, CRC Press, 2011.
[38] C. Hofstetter, S. Orman, S. Baudis, J. Stampfl, Combining cure depth and cure degree, a new way to fully characterize novel photopolymers, Addit. Manuf. 24 (2018) 166–172, https://doi.org/10.1016/j.addma.2018.09.025.
[39] Y. Yang, L. Li, J. Zhao, Mechanical property modeling of photosensitive liquid resin in stereolithography additive manufacturing: bridging degree of cure with tensile strength and hardness, Mater. Des. 162 (2019) 418–428, https://doi.org/10.1016/j.matdes.2018.12.009.
[40] G. Mitteramskogler, R. Gmeiner, R. Felzmann, S. Gruber, C. Hofstetter, J. Stampfl, J. Ebert, W. Wachter, J. Laubersheimer, Light curing strategies for lithography-based additive manufacturing of customized ceramics, Addit. Manuf. 1-4 (2014) 110–118, https://doi.org/10.1016/j.addma.2014.08.003.
[41] C.I. Fiedler-Higgins, L.M. Cox, F.W. DelRio, J.P. Killgore, Monitoring fast, voxel-scale cure kinetics via sample-coupled-resonance photorheology, Small Methods 3 (2) (2019) 1800275, https://doi.org/10.1002/smtd.201800275.
[42] M.M. Emami, F. Barazandeh, F. Yaghmaie, Scanning-projection based stereolithography: method and structure, Sens. Actuators A: Phys. 218 (2014) 116–124, https://doi.org/10.1016/j.sna.2014.08.002.
[43] S. Westbeek, J.A.W. van Dommelen, J.J.C. Remmers, M.G.D. Geers, Multiphysical modeling of the photopolymerization process for additive manufacturing of ceramics, Eur. J. Mech. A/Solids 71 (2018) 210–223, https://doi.org/10.1016/j.euromechsol.2018.03.020.
[44] T. Chartier, C. Dupas, P.-M. Geffroy, V. Pateloup, M. Colas, J. Cornette, S. Guillemet-Fritsch, Influence of irradiation parameters on the polymerization of ceramic reactive suspensions for stereolithography, J. Eur. Ceram. Soc. 37 (15) (2017) 4431–4436, https://doi.org/10.1016/j.jeurceramsoc.2017.05.050.
[45] J. Bennett, Measuring UV curing parameters of commercial photopolymers used in additive manufacturing, Addit. Manuf. 18 (2017) 203–212, https://doi.org/10.1016/j.addma.2017.10.009.